Atomic structure of $As_{25}Si_{40}Te_{35}$ glass

2007 J. Phys.: Condens. Matter 19 335210

(http://iopscience.iop.org/0953-8984/19/33/335210)

IOP PUBLISHING JOURNAL OF PHYSICS: CONDENSED MATTER

J. Phys.: Condens. Matter **19** (2007) 335210 (9pp) doi:10.1088/0953-8984/19/33/335210

Atomic structure of $As_{25}Si_{40}Te_{35}$ glass

I Kaban[1,5], S Gruner[1], P Jóvári[2], M Kehr[1], W Hoyer[1], R G Delaplane[3] and M Popescu[4]

[1] Institute of Physics, Chemnitz University of Technology, D-09107 Chemnitz, Germany
[2] Research Institute for Solid State Physics and Optics, H-1525 Budapest, POB 49, Hungary
[3] Borgdalsgangen 36, SE-61157 Nyköping, Sweden
[4] National Institute of R&D for Materials Physics, 76900-Bucharest-Magurele, PO Box MG. 7, Romania

E-mail: ivan.kaban@physik.tu-chemnitz.de

Received 21 February 2007
Published 4 July 2007
Online at stacks.iop.org/JPhysCM/19/335210

Abstract

Glassy $As_{25}Si_{40}Te_{35}$ has been studied by x-ray and neutron diffraction as well as x-ray absorption spectroscopy (EXAFS) at As and Te K-edges. Simultaneous modelling of the four independent measurements by means of the reverse Monte Carlo (RMC) simulation technique allowed the separation of partial pair distribution functions and estimation of the corresponding coordination numbers. It is shown that the atomic structure of $As_{25}Si_{40}Te_{35}$ glass can be presented as a three-dimensional network of twofold coordinated Te, threefold coordinated As and fourfold coordinated Si atoms.

1. Introduction

The ternary As–Si–Te system exhibits high interest in view of both basic physics and technological applications. Due to the combination of elements of different valences, this system is characterized by a very large glass formation region with a wide controllability range of physical properties such as the glass transition temperature, electrical and optical energy gaps etc [1–5]. From a technological point of view, amorphous As–Si–Te could be applied to multilayered heterojunction devices and optoelectronic functional elements. These glasses are also suitable for high-temperature applications because of a high glass transition temperature. An advantage of the As–Si–Te alloys is that this material can easily be deposited on any inexpensive substrate such as glass, ceramics or metal surfaces.

The relation between the switching parameters and other properties of multicomponent chalcogenide glasses including the As–Si–Te system (e.g. between the switching voltage and the glass transition temperature, crystallization temperature, electrical resistivity etc) has been studied extensively so far. It is known that some properties of amorphous As–Si–Te depend

[5] Author to whom any correspondence should be addressed.

strongly on the composition. For example, the electric-conduction activation energy of these glasses changes from 0.6 to 1.5 eV [6]. It is supposed that the electrical conductivity is affected by Si-containing structural units in amorphous As–Si–Te alloys.

However, still little is known about the relation between the physical properties and the structure of amorphous chalcogenides, especially those containing three or more components. The latter is not well investigated and elucidated, since an understanding of the structure of multicomponent alloys requires knowledge of the partial atomic distributions, which are hard to obtain experimentally. Often it is difficult (if possible at all) to perform the necessary number of independent diffraction experiments. The reverse Monte Carlo simulation method [7] enables one to obtain the partial distribution functions of a multicomponent alloy from a reduced number of experimental data. It has been shown in [8, 9], for example, that in favourable cases it is possible to get a set of reliable partial pair distribution functions for a binary alloy from two independent scattering experiments (x-ray diffraction and neutron diffraction). Furthermore, RMC can be used as a tool to combine diffraction and EXAFS data within one simulation run.

In this work we study the local atomic structure in amorphous $As_{25}Si_{40}Te_{35}$, which is situated near the composition $As_2Te_4Si_4$, exhibiting one of the highest softening temperatures in the glass domain of the As–Si–Te ternary system [1]. We performed x-ray diffraction (XRD), neutron diffraction (ND) and EXAFS measurements at the As and Te K-edges and analysed them with the RMC.

2. Experimental details

The amorphous alloy $As_{25}Si_{40}Te_{35}$ was prepared from pure As (99.999%), Si (99.999%) and Te (99.99%). Appropriate amounts of the components were mixed and sealed in a quartz ampoule under a pressure of $\sim$1 mbar. The ampoule was heated up to 950 °C and kept for 24 h. After homogenization, the sample was quenched in water.

The neutron diffraction was performed with the liquid and amorphous materials diffractometer SLAD at the Studsvik Neutron Research Laboratory (NFL), Studsvik, Sweden [10]. The powdered sample was contained in a thin-walled vanadium container. The incident wavelength of neutrons was 1.11 Å. The scattered intensity was measured between 0.4 and 10.4 $Å^{-1}$. The static structure factor was obtained from the scattering intensities after applying corrections for absorption, multiple scattering and inelasticity followed by normalization to a vanadium standard, which was done with the CORRECT program described in [11].

X-ray diffraction was carried out at the BW5 experimental station [12] at HASYLAB, DESY, Hamburg, Germany. The sample material was filled into a thin-walled (0.02 mm) quartz capillary of 2.0 mm in diameter. The energy of the incident beam was 99.8 keV. The size of the incident beam was 1×4 mm^2. Raw data were corrected for background, polarization, detector dead-time and variations in detector solid angle.

The EXAFS measurements were carried out at the beam lines A1 (As K-edge) and X1 (Te K-edge) of HASYLAB in transmission mode. The sample was finely ground, mixed with cellulose powder and pressed into tablets. The sample quantity in the tablets was adjusted to the composition of the sample and to the selected edge.

3. RMC modelling

The XRD, ND and EXAFS experimental data for $As_{25}Si_{40}Te_{35}$ glass were modelled simultaneously in the framework of the reverse Monte Carlo simulation technique [7]. The aim of the RMC modelling procedure is to generate a three-dimensional arrangement of atoms

that reproduces the experimental total structure factors, EXAFS modulation curves as well as the constraints given. This is achieved by modifying an initial configuration with the number density, ρ_0, by random atomic moves. After each move, the partial pair distribution functions are determined by counting the number $n_{ij}(r)$ of j-type neighbours in a shell with thickness Δr at the distance r around a chosen central atom of type i and averaging over all i atoms within the configuration:

$$g_{ij}^{\mathrm{RMC}}(r) = \frac{\langle n_{ij}(r)\rangle}{4\pi\rho_0 r^2 \cdot \Delta r}. \tag{1}$$

To evaluate the diffraction data, the partial pair distribution functions obtained from the RMC configuration are transformed into the Q-space, yielding partial structure factors $S_{ij}^{\mathrm{RMC}}(Q)$, which can be combined into the model total Faber–Ziman structure factor [13]

$$S^{\mathrm{RMC}}(Q) = \sum_{i,j} w_{ij}(Q) S_{ij}^{\mathrm{RMC}}(Q), \qquad w_{ij}(Q) = \frac{c_i c_j f_i(Q) f_j(Q)}{\langle f(Q)\rangle^2}, \tag{2}$$

where the factors $f_i(Q)$ represent the Q-dependent atomic form factors for x-ray diffraction and are to be substituted by the coherent scattering lengths b_i for neutron diffraction.

The model EXAFS modulation can be obtained from the model pair distribution functions by applying the expression [14]

$$X_i^{\mathrm{RMC}}(k) = 4\pi\rho_0 \sum_j c_j \int_0^R \mathrm{d}r\, r^2 \gamma_{ij}(r,k) g_{ij}^{\mathrm{RMC}}(r), \tag{3}$$

where i denotes the absorbing species.

The EXAFS backscattering coefficients γ_{ij} of the atomic pairs consisting of phase and amplitude factors were determined in this work using the FEFF8-code [15] in the SCF (self-consistent field) approximation. The contributions involving more than one backscattering atom were neglected during the calculation of the backscattering signals, since the RMC uses the pair distribution function formalism. As the EXAFS signal is strongly damped due to the limited mean free path of the electrons emitted during the absorption process, the integration limit R in equation (3) has been chosen to contain only the first coordination shell.

Because of the phase shift of the backscattered electrons, the peaks in $X(r)$—the Fourier transform of $X(k)$—do not correspond to real r-space distances. Therefore $X(r)$ can be obtained from the partial pair distribution functions in two steps only: first $X(k)$ should be calculated from the corresponding $g_{ij}(r)$ functions according to equation (3) and then $X(k)$ should be transformed to $X(r)$. For this reason the fit to the experimental data has been carried out in the reciprocal space.

The difference between the experimental functions $S^{\mathrm{exp}}(Q)$ and $X^{\mathrm{exp}}(k)$ (or, in most cases, $k^n X^{\mathrm{exp}}(k)$, $n = 2, 3$) and those derived from the RMC model is calculated using the expression [14]

$$\chi^2 = \sum_\alpha \frac{1}{\sigma_k^2} \sum_i [S^{\mathrm{RMC},\alpha}(Q_i) - S^{\mathrm{exp},\alpha}(Q_i)]^2 + \sum_\beta \frac{1}{\sigma_l^2} \sum_i [k_i^n X_\beta^{\mathrm{RMC}}(k_i) - k_i^n X_\beta^{\mathrm{exp}}(k_i)]^2. \tag{4}$$

If the value of χ^2 has increased after moving an atom, this move is accepted with the probability

$$P \sim \exp\left(-\frac{\chi^2_{\mathrm{new}} - \chi^2_{\mathrm{old}}}{2}\right). \tag{5}$$

On the other hand, all moves leading to a reduction in χ^2 are accepted. Thus, in an iterative process the fit between the experimental and the model functions is improved, but being trapped

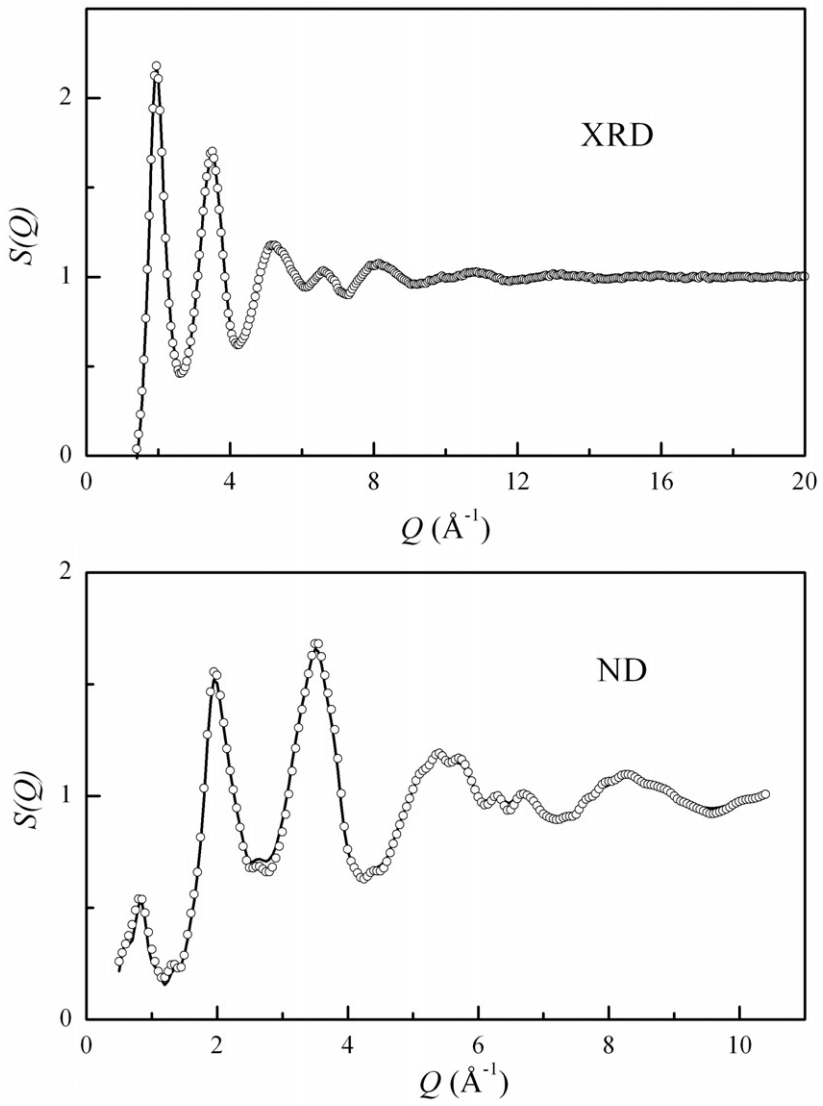

Figure 1. The experimental (*circles*) XRD and ND structure factors for amorphous $As_{25}Si_{40}Te_{35}$ compared to the RMC fits (*lines*) obtained by simultaneous simulation of the XRD, ND and EXAFS data under application of the coordination constraints: $\langle N_{As} \rangle = 3$, $\langle N_{Si} \rangle = 4$.

in local minima is avoided. The parameters σ_l substitute the temperature within the framework of Monte Carlo modelling algorithms and thus regulate the impact that an individual data-set has on the whole simulation.

4. Results and discussion

The experimental XRD and ND structure factors for amorphous $As_{25}Si_{40}Te_{35}$ are plotted in figure 1, while the experimental $k^3X(k)$ EXAFS curves obtained at As and Te K-edges are shown in figure 2.

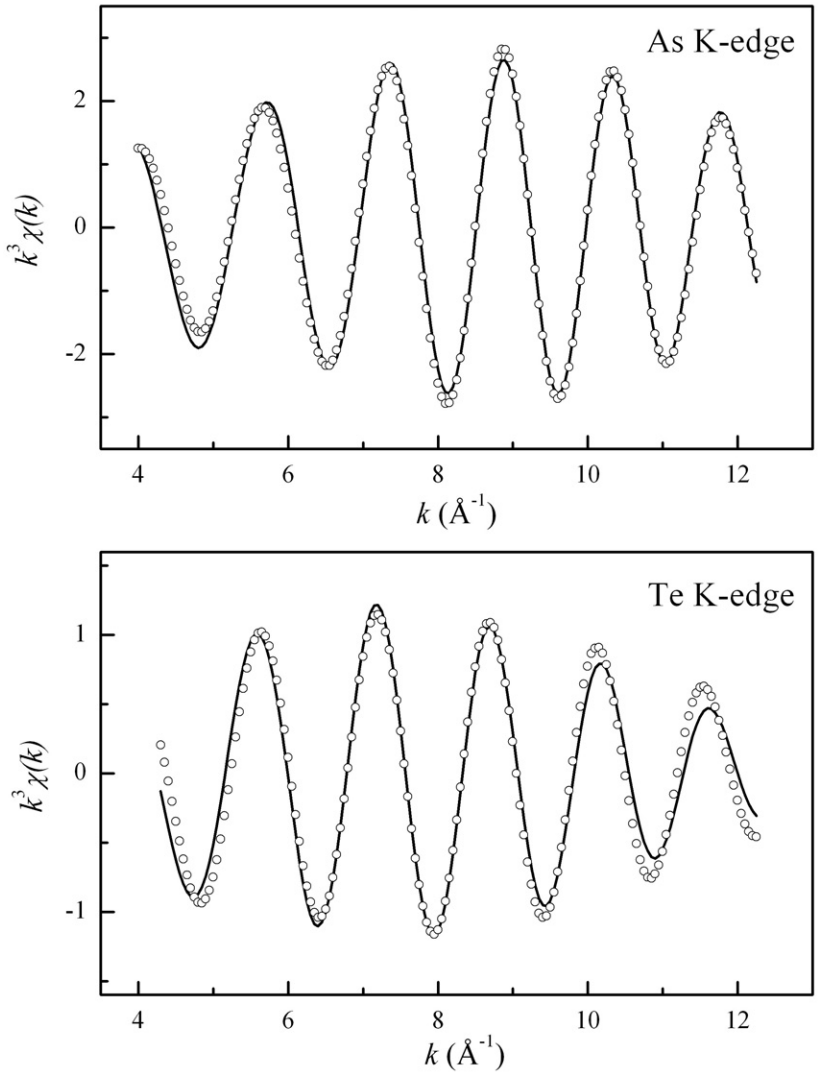

Figure 2. The experimental (*circles*) As and Te K-edge $k^3X(k)$ curves for amorphous $As_{25}Si_{40}Te_{35}$ compared to the RMC fits (*lines*) obtained by simultaneous simulation of the XRD, ND and EXAFS data under application of the coordination constraints: $\langle N_{As}\rangle = 3$, $\langle N_{Si}\rangle = 4$.

The atomic density $\rho_0 = 0.033\,65$ Å^{-3} is used throughout the RMC simulations. This has been calculated from the experimental mass density of the $As_{25}Si_{40}Te_{35}$ glass prepared in the same way as our sample and studied in [16]. The modelling was started with a random configuration of 500 atoms, where the distances of closest approach for all pairs were fixed to be 1.8 Å (enough below the respective sums of the covalent radii) and a rough fit to the diffraction data was obtained. The partial pair distribution functions derived from this configuration showed distinct first maxima and allowed us to choose the following minimum interatomic distances: $r_{AsAs} = 2.2$ Å, $r_{AsTe} = 2.4$ Å, $r_{AsSi} = 2.1$ Å, $r_{SiSi} = 2.2$ Å and $r_{SiTe} = 2.3$ Å. Analysis of the fits and partial pair distribution functions showed that the diffraction data do not support direct Te–Te neighbours, therefore $r_{TeTe} = 3.1$ Å was chosen. This (the absence

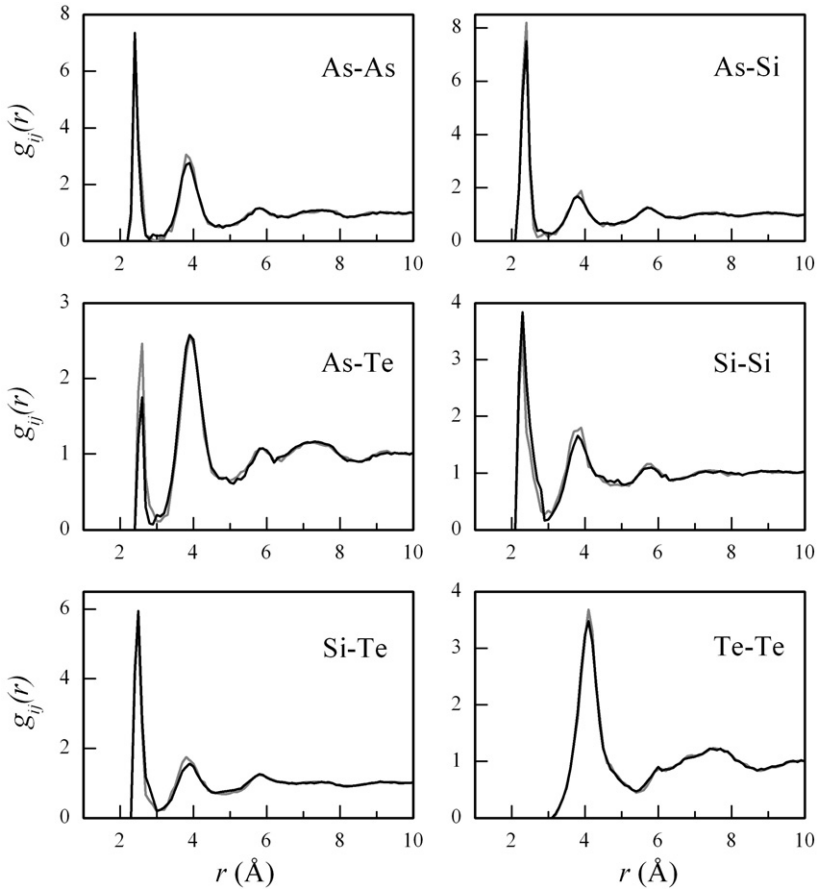

Figure 3. RMC simulated partial pair distribution functions for glassy $As_{25}Si_{40}Te_{35}$: *grey*—without coordination constraints; *black*—with the constraints $\langle N_{As}\rangle = 3$, $\langle N_{Si}\rangle = 4$.

of direct Te–Te bonds) correlates with the results of Raman spectrometry carried out in [16], where no Te–Te band was found. No coordination constraints were applied at this stage of modelling.

After the first runs the box size was doubled in each direction. With this configuration, the XRD and ND diffraction experiments and both EXAFS curves were fitted simultaneously by reducing the parameters σ_l stepwise. Finally, the box size was again increased to 32 000 atoms, mainly to achieve good counting statistics when determining the $g_{ij}(r)$ following equation (1).

The partial pair distribution functions $g_{ij}(r)$ calculated from the unconstrained model are plotted in figure 3. A remarkable feature of all $g_{ij}(r)$ functions is a pronounced separation of the first and second coordination spheres. This is obviously due to strong covalent bonding in the alloy studied. The values of the mean inter-atomic distance r_{ij} and the coordination numbers N_{ij} obtained from the partial pair distribution functions $g_{ij}(r)$ are given in tables 1 and 2, respectively. The partial coordination numbers have been calculated by integrating $4\pi r^2 \rho_0 c_j g_{ij}(r)$ from the left-hand edge of the first peak to the first minimum in the pair distribution function.

Technologically important glasses often consist of three or more components. For such complicated systems, detailed structural information can only be obtained by the combination

Table 1. The mean nearest-neighbour distances r_{ij} for amorphous $As_{25}Si_{40}Te_{35}$. The uncertainty of r_{ij} is ± 0.03 Å.

Pair ij	As–As	As–Si	As–Te	Si–Si	Si–Te
r_{ij} (Å) (without CN constraints)	2.43	2.38	2.58	2.36	2.49
r_{ij} (Å) (with constraint: $\langle N_{Te}\rangle = 2$)	2.43	2.38	2.58	2.37	2.52
r_{ij} (Å) (with constraints: $\langle N_{As}\rangle = 3$, $\langle N_{Si}\rangle = 4$)	2.42	2.38	2.57	2.38	2.50

Table 2. Coordination numbers N_{ij} for amorphous $As_{25}Si_{40}Te_{35}$. The error of unconstrained coordination numbers is about 10%.

Pair ij	As–As	As–Si	As–Te	Si–Si	Si–As	Si–Te	Te–As	Te–Si
N_{ij} (without CN constraints)	0.86	1.84	0.57	1.07	1.15	1.33	0.40	1.52
N_{ij} (with constraint $\langle N_{Te}\rangle = 2$)	0.86	1.85	0.59	1.02	1.16	1.37	0.37	1.57
N_{ij} (with constraints $\langle N_{As}\rangle = 3$, $\langle N_{Si}\rangle = 4$)	0.82	1.82	0.32	1.38	1.13	1.50	0.23	1.71

of different techniques. It is interesting to see the depth of results that can be obtained from available experimental data. Though there are some factors influencing the reliability of models in an uncontrollable way (e.g. systematic errors), still in most cases a rough estimate can be given.

The resolution (i.e. the *bin size* in r-space needed to reproduce the data in Q-space after Fourier transformation) of a diffraction measurement is given by $\delta r = \pi/(Q_{max} - Q_{min})$. It is not to be mixed with the formula connecting *lattice spacing* and Q values ($d = 2\pi/Q$). The latter can be used for crystalline materials, while the first expression is valid for both periodic and non-periodic systems. The resolution also gives the number of free parameters in a fitting procedure. If the width of an r-space feature is ΔR, then the number of bins (and the number of free parameters) is given by $\Delta R/\delta r$. The resolution of an EXAFS dataset is $\pi/2(k_{max} - k_{min})$. The physical background of the difference is that the backscattered photoelectron travels twice between the absorber and the backscatterer, thus the phase-shift formula contains $2kr$ and not simply kr, as for diffraction. In the case of multiple (and non-degenerate) data-sets, the number of free parameters is summed up. We try to decompose five overlapping peaks between 2.1 and 3.0 Å. Over this range the total number of free parameters is $\sim$17 in our case. Additional information can be incorporated into the fitting by applying different cut-offs for different atoms (this way, for example, $g_{AsTe}(r)$ is forced to be 0 for $r \leqslant 2.4$ Å). The situation can be improved further by incorporating *a priori* chemical knowledge in the modelling (e.g. by constraining the coordination number of an element). These features of the RMC are exploited in this study, as this will be seen further.

The combination of available experimental information with real-space constraints thus allows us to determine bond lengths and coordination numbers. The error of these quantities depends most strongly on two main factors: (1) the weight of a given partial $g_{ij}(r)$ function in experimental data—the error is certainly larger in case of weakly scattering or low-

concentration species; (2) due to a correlation between coordination numbers and peak positions, the separation of $g_{ij}(r)$s is also difficult if there are components with similar size and scattering power.

The error in the bond lengths is about ± 0.03 Å. Possible sources of the error are mainly peak shape asymmetry and inaccuracy of backscattering amplitudes. The only exception is the mean Si–Si distance. As Si scatters weakly, both x-ray and neutron diffraction measurements are not quite sensitive to Si–Si correlations. Here the estimated uncertainty is about ± 0.06 Å.

The uncertainty in total coordination numbers is about 5–10%, and this can be considered to be a lower limit of the error in (partial) coordination numbers obtained by unconstrained simulations. The uncertainty in coordination numbers can be decreased by using constraints (e.g. forcing As to be threefold coordinated—see below). It should also be mentioned that the average coordination numbers obtained by RMC simulation do not necessarily mean that all atoms of a respective constituent element have the same number of nearest neighbours. As RMC tends to produce the most disordered configuration compatible with the experimental data and constraints, the distribution of coordination numbers can be broad (e.g. along with twofold-coordinated Te, there can be Te atoms with one, three or four neighbours as well). If there is a special interest in atomic configuration and coordinates, these 'defects' can be eliminated by using some special constraints in the simulation. It was, however, beyond the scope of the present study, where atomic structure at the level of pair distribution functions is analysed.

The average numbers of atoms around As, $\langle N_{\mathrm{As}} \rangle = 3.3 \pm 0.3$, around Si, $\langle N_{\mathrm{Si}} \rangle = 3.6 \pm 0.4$ and around Te, $\langle N_{\mathrm{Te}} \rangle = 1.9 \pm 0.2$, were obtained without coordination constraints. In general, these values correlate rather well with the usual coordination of As (3), Si (4) and Te (2). However, As appeared to be overcoordinated, while Si is undercoordinated.

At the next step we performed RMC simulations with a constrained coordination number of Te ($\langle N_{\mathrm{Te}} \rangle = 2$). Other parameters remained unchanged. The coordination numbers obtained are given in tables 1 and 2. The mean interatomic distances for most pairs are the same as those obtained in the 'unconstrained' simulations, and only the Si–Te bond distance has slightly increased from 2.49 to 2.52 Å. The coordination numbers are not changed. This suggests that As and Si are mixed if they are not constrained: $\langle N_{\mathrm{As}} \rangle$ is larger than three, while $\langle N_{\mathrm{Si}} \rangle$ is smaller than four.

Therefore we carried out further simulations, where the coordination numbers for As and Si atoms were constrained to be three and four, respectively. The minimum interatomic distances were the same as in the previous runs. The simulated total structure factors and $k^3X(k)$ curves are compared with the respective experimental functions in figures 1 and 2. The partial pair distribution functions, $g_{ij}(r)$, are plotted in figure 3. The values of r_{ij} and N_{ij} obtained are listed in tables 1 and 2. Also, in this case the mean interatomic distances are practically the same as those obtained in the previous simulation runs. However, the coordination numbers reached their expected values, namely: $\langle N_{\mathrm{As}} \rangle = 3.0$, $\langle N_{\mathrm{Si}} \rangle = 4.0$ and $\langle N_{\mathrm{Te}} \rangle = 1.9 \pm 0.2$. (As $\langle N_{\mathrm{As}} \rangle$ and $\langle N_{\mathrm{Si}} \rangle$ are not free parameters, we do not give errors for them.) It is noteworthy that the number of Si neighbours has been increased in the 'As and Si constrained' case, mostly due to the building of additional Si–Te and Si–Si bonds. At the same time, As atoms lost nearly half of their Te neighbours, while As–As and As–Si pairs were preserved. It appears from the results of RMC modelling that As and Te atoms try to avoid each other in amorphous $As_{25}Si_{40}Te_{35}$. Even in the 'unconstrained' case the As–Te and Te–As coordination numbers were the lowest. The highest coordination numbers show As–Si, Si–Te and Si–Si pairs (table 2). These findings correlate very well with values of the single covalent bond energies estimated in [4]. They are 53.4, 50.49, 43.81, 43.4, 38.61 and 34.0 kcal mol^{-1} for Si–Si, Si–As, Si–Te, As–As, As–Te and Te–Te pairs, respectively.

The average coordination number ($\langle N\rangle = 0.25\langle N_{\mathrm{As}}\rangle + 0.40\langle N_{\mathrm{Si}}\rangle + 0.35\langle N_{\mathrm{Te}}\rangle$) obtained in the second 'constrained' case is 3.0 ± 0.1. This value is higher than the characteristic parameter of topological phase transition in chalcogenide glasses ($\langle N\rangle = 2.67$) suggested by Tanaka [17] and therefore indicates a three-dimensional network structure in glassy $As_{25}Si_{40}Te_{35}$.

Srinivasan *et al* [3, 4] suggested that $AsTe_{3/2}$ and $SiTe_{4/2}$ are the basic structural units of As–Si–Te glasses. As follows from the results obtained in our study, the network structure of glassy $As_{25}Si_{40}Te_{35}$ cannot be described simply by the $AsTe_{3/2}$ and $SiTe_{4/2}$ units.

5. Conclusions

Simultaneous reverse Monte Carlo simulation of the x-ray and neutron diffraction data with the EXAFS spectra measured at As and Te K-edges on glassy $As_{25}Si_{40}Te_{35}$ has been carried out. Several simulation runs with different constraints were analysed. At the end, the combination of the four independent measurements and use of some plausible coordination constraints allowed separation of the partial pair distribution functions. The atomic structure of amorphous $As_{25}Si_{40}Te_{35}$ can be presented as a three-dimensional network of threefold-coordinated As, fourfold-coordinated Si and twofold-coordinated Te atoms. Si–Si and As–As bonding was found to be significant. The latter excludes the predominance of $AsTe_{3/2}$ units in $As_{25}Si_{40}Te_{35}$. On the other hand, Te is coordinated mostly by Si.

Acknowledgments

IK and MK acknowledge Deutsches Elektronen-Synchrotron (DESY) for financial support. PJ was supported by the OTKA (Hungarian Basic Research Found) grant no. T048580.

References

[1] Savage J A 1972 *J. Mater. Sci.* **7** 64
[2] Kastner M 1973 *Phys. Rev.* B **7** 5237
[3] Srinivasan A, Ganesan R, Madhusoodanan K N and Gopal E S R 1992 *J. Mater. Sci. Lett.* **11** 1698
[4] Srinivasan A, Madhusoodanan K N, Gopal E S R and Philip J 1993 *J. Non-Cryst. Solids* **155** 267
[5] Hamakawa Y 1994 *Proc. 1st World Conf. on PV Energy Conversion (Waikoloa, Hawai)* p 1
[6] Borisova Z U 1981 *Glassy Semiconductors* (New York: Plenum)
[7] McGreevy R L and Pusztai L 1988 *Mol. Simul.* **1** 359
[8] Kaban I, Gruner S, Hoyer W, Jóvári P, Delaplane R G and Wannberg A 2005 *Phys. Chem. Glasses* **46** 472
[9] Gruner S, Akinlade O and Hoyer W 2006 *J. Phys.: Condens. Matter* **18** 4773
[10] Wannberg A, Mellergård A, Zetterström P, Delaplane R, Grönros M, Karlsson L-E and McGreevy R L 1999 *J. Neutron Res.* **8** 133
[11] Howe M A, McGreevy R L and Zetterström P 1996 *CORRECT: A Correction Program for Neutron Diffraction Data (NFL Studsvik Internal Report)*
[12] Poulsen H, Neuefeind J, Neumann H B, Schneider J R and Zeidler M D 1995 *J. Non-Cryst. Solids* **188** 63
[13] Faber T E and Ziman J M 1965 *Phil. Mag.* **11** 153
[14] Gurman S J and McGreevy R L 1990 *J. Phys.: Condens. Matter* **2** 9463
[15] Ankudinov A L, Ravel B, Rehr J J and Conradson S D 1998 *Phys. Rev.* B **58** 7565
[16] Lörinczi A, Sava F, Iovu M, Leonovici M, Halm Th, Popescu M and Hoyer W 2003 *Phys. Status Solidi* b **240** 29
[17] Tanaka K 1988 *Phys. Rev.* B **39** 1270